Glycine radicals in the gas phase †‡

František Tureček * and F. Howland Carpenter

Department of Chemistry, Bagley Hall, Box 351700, University of Washington, Seattle, WA 98195-1700, USA

Received (in Cambridge, UK) 18th May 1999, Accepted 17th June 1999

2-Glycyl radical (**1**), 2-glycyl methyl ester (**2**), and 2-glycyl *N*-methylamide radicals (**3**) were generated in the gas phase by collisional neutralization of the corresponding cations and studied by neutralization–reionization (NR) mass spectrometry and *ab initio* and density functional theory calculations. Stable fractions were found for **1**–**3** that did not dissociate on the 4 μs timescale of the experiment. The major unimolecular dissociations observed were cleavages of the CO–X bonds (X = OH, OCH_3, and $NHCH_3$) to form aminoketene, and cleavages of the C–CO bond to form aminocarbene, which gave rise to prominent fragments in the NR mass spectra. In addition, hydrogen rearrangements occurred in **1**–**3** and an unusual methyl migration took place in **3**. G2(MP2) bond dissociation energies are reported for **1** and $\mathbf{1}^+$. Combined B3LYP and PMP2/6-311+G(2df,p) calculations were used to provide bond dissociation energies for **2**, $\mathbf{2}^+$, **3** and $\mathbf{3}^+$.

Introduction

In the last decade several enzymatic systems have been discovered that produced reactive radical intermediates in proteins.[1] In addition to tyrosyl radicals,[2–4] and tryptophan radicals,[5–7] attention has been focused recently on carbon-centered radicals formed transiently in glycine residues by the action of pyruvate formate lyase[8,9] and anaerobic ribonucleotide reductases.[10–12] The properties of glycine radicals have been studied by electron paramagnetic resonance spectroscopy both for free glycine[13] and for glycine residues in proteins.[14,15] In addition, computational studies of glycine radicals have been reported that established the most stable radical tautomers[16] and predicted the magnitude of hyperfine splittings in the EPR spectra.[17–19]

Since glycine radicals are transient species, questions arise about their intrinsic stability in the peptide chain. In addition to hydrogen atom transfer reactions, which are thought to constitute an important step in the enzyme-induced reaction,[20] the radicals may undergo undetected side reactions, such as peptide chain breaks. Such reactions are difficult to identify by EPR. The intrinsic properties of carbon-centered glycine radicals are therefore of interest.

Neutralization–reionization mass spectrometry (NRMS)[21] is the method of choice for the generation of transient species in the gas phase where they can be studied in the absence of solvent, oxygen, salts, and other components commonly present in the biological fluid. NRMS relies on the generation of a gas-phase ion that has the same chemical structure as the neutral species of interest (Scheme 1). The ion is selected by the mass-to-charge ratio (*m*/*z*), accelerated to a high velocity corresponding to a kinetic energy in the kiloelectron volt range, and discharged by a glancing collision with a suitable gaseous target. For an ion travelling at 150 000 m s^{-1}, the electron transfer during the collision lasts a few femtoseconds, which ensures that the nascent fast neutral species has the exact structure of the precursor ion. The properties of transient molecules or radicals prepared by femtosecond electron transfer are then interrogated on a microsecond timescale through unimolecular dissociations, collisional activation,[22–24] kinetic measurements (variable-time NRMS),[25–27] or laser photoexcitation.[28–30] Surviving radicals and products of radical dissociations are then ionized by a glancing collision and analyzed by mass spectrometry.

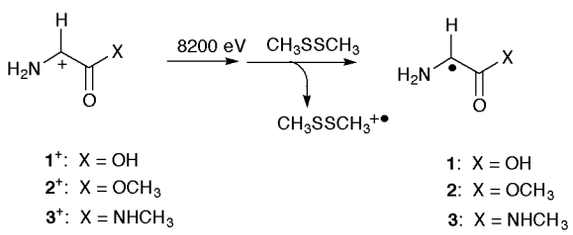

Scheme 1

In this work we report on the preparation of gas-phase radicals derived from glycine (**1**),[31] glycine methyl ester (**2**) and glycine *N*-methylamide (**3**). These radicals can be thought of as simple models of peptides containing glycyl radical residues. In addition, the structures of glycyl cations and radicals and the energetics of their unimolecular dissociations are examined with *ab initio* and density functional theory calculations.

Experimental

Materials

Phenylalanine and phenylalanine methyl ester hydrochloride were purchased from Sigma and used as received. Phenylalanine *N*-methylamide was prepared by treating phenylalanine methyl ester hydrochloride with a 10-fold molar excess of 40% aqueous methylamine at room temperature for 24 h. The solvent was evaporated *in vacuo* and the crude product was characterized by the electron-impact mass spectrum that showed peaks at *m*/*z* 161, 160, 120, 103, 91, 87, 77, 69, 58, 42, and 30. *N*-(Phenylalaninyl)pyrrolidine was prepared by treating phenylalanine methyl ester hydrochloride with 10-fold molar excess of pyrrolidine at 40 °C for 12 h. The solvent was evaporated *in vacuo* and the crude product was characterized by the electron impact mass spectrum which showed peaks at *m*/*z* 127, 120, 112, 103, 91, 70, 59 and 43. Deuterium-labeled derivatives were prepared by dissolving the phenylalanine derivatives (500 mg) in 5 mL of a 1:1 mixture of D_2O and CH_3OD and stirring for 1 h. The solvents were then evaporated at room temperature

† Dedicated to the memory of Robert R. Squires.

‡ Tables of total energies and zero-point corrections are available as supplementary data. For direct electronic access see http://www.rsc.org/suppdata/p2/1999/2315, otherwise available from BLDSC (SUPPL. NO. 57627, pp. 4) or the RSC Library. See Instructions for Authors available *via* the RSC web page (http://www.rsc.org//authors).

with a stream of dry nitrogen and the deuterated product was sampled into the mass spectrometer. The direct inlet system and the ion source were conditioned with 10^{-5} Torr D_2O for at least 30 min before the measurements and D_2O was also admitted in the ion source during the measurements.

Methods

Neutralization–reionization mass spectra were obtained on a home-built tandem quadrupole acceleration deceleration mass spectrometer which was described in detail previously.[32] Samples were introduced into the ion source from a heated glass solid probe of our design. Typical conditions for electron ionization were as follows: electron energy 70 eV, electron current 500 μA, ion energy 70 eV, and source temperature 230–270 °C. The ions were extracted from the source and passed through a quadrupole operated in the radiofrequency only mode. A series of lenses accelerated the ions and the final translational energy was 8250 eV. The fast ions entered a collision cell in which dimethyl disulfide was introduced as a neutralization gas to achieve 70% transmittance (T) of the precursor ion current. At this transmittance, >85% of the colliding ions underwent single collisions. The neutrals and ions exited the collision cell and entered the conduit region. The fast ions were deflected by the first element of the conduit which was floated at +250 V while the neutrals passed unhindered. The lifetimes of the neutrals in the 60 cm long conduit were 4.1, 4.5, and 4.4 μs for **1**, **2**, and **3**, respectively. The surviving neutrals and fragments were then reionized in a second collision cell by O_2 introduced to achieve 70% T of the precursor ion current. The fast ions were decelerated to 80 eV translational energy, energy filtered, mass analyzed by a second quadrupole, and detected by an off-axis electron multiplier. The signal was converted to a voltage and amplified by a Keithley 428 amplifier. A series of scans, usually 20–30, were collected and processed by a PC based control system.

Collisionally activated dissociations (CAD) were performed in the first field-free region of a JEOL-HX100 double-focusing mass spectrometer using linked B/E scans. Air was used as the collision gas at 50 and 70% T of the precursor ion beam.

2.2. Calculations. Standard *ab initio* and density functional theory calculations were performed using the GAUSSIAN94 suite of programs.[33] Geometries were optimized using Becke's hybrid functional (B3LYP)[34,35] and the 6-31+G(d,p) basis set. Basis sets of this quality have been shown to give mostly reliable equilibrium geometries for neutral molecules and ions.[36] The optimized structures were characterized by harmonic frequency analysis as local minima (all frequencies real) or first-order saddle points (one imaginary frequency). The B3LYP/6-31+G(d,p) frequencies were scaled by 0.961 (ref. 37, for other scaling factors see refs. 38–40) and used to calculate zero-point energies and enthalpy corrections. Single-point energies were calculated at three levels of theory. Møller–Plesset theory[41] truncated at second order with frozen-core excitations (MP2) was used with the 6-311+G(2df,p) basis set to obtain a set of single-point energies. In addition, B3LYP calculations were performed with the 6-311+G(2df,p) basis set. At the highest level of theory, GAUSSIAN-2(MP2) calculations[42–44] were performed for selected species using the B3LYP/6-31+G(d,p) optimized geometries and zero-point corrections. This consisted of MP2/6-311+G(3df,2p), MP2/6-311G(d,p), and QCISD(T)/6-311G(d,p) calculations which were combined to provide effective QCISD(T)/6-311+G(3df,2p) energies.

Results and discussion

Ion dissociations

Precursor cations for the generation of glycine radicals were prepared by dissociative ionization of phenylalanine derivatives. In particular, phenylalanine dissociated upon electron impact ionization by eliminating the benzyl group to yield an abundant NH_2–CH–$COOH^+$ ion at *m/z* 74 (**1**$^+$).[31] Likewise, upon electron impact phenylalanine methyl ester, phenylalanine *N*-methylamide, and *N*-(phenylalanyl)pyrrolidine eliminated benzyl groups to form ions **2**$^+$ (*m/z* 88), **3**$^+$ (*m/z* 87), and **4**$^+$ (*m/z* 127), respectively, (Scheme 2). Deuterium-labeled ions

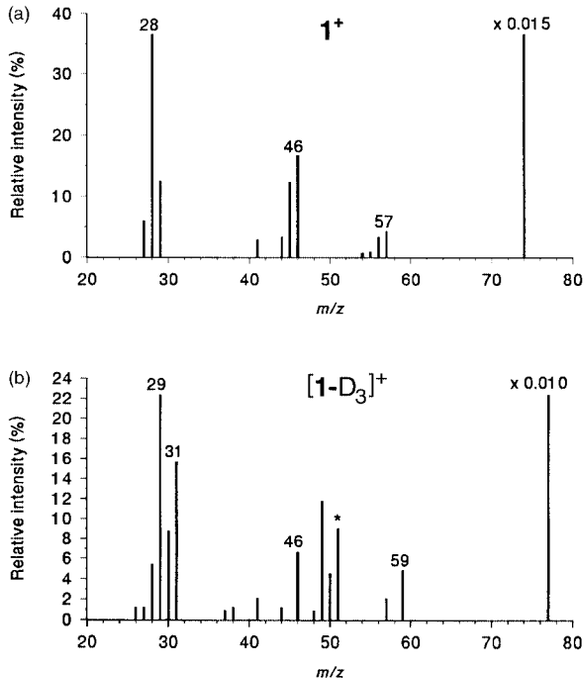

Fig. 1 Collisionally-activated spectrum of (a) **1**$^+$, (b) [**1**-D_3]$^+$. The ion relative intensities were normalized to the sum of CAD intensities.

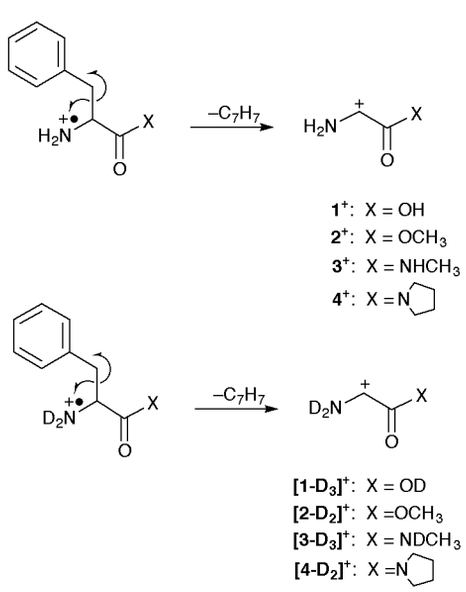

Scheme 2

[**1**-D_3]$^+$, [**2**-D_2]$^+$, [**3**-D_3]$^+$, and [**4**-D_2]$^+$, were prepared from phenylalanine derivatives in which the active hydrogen atoms were exchanged for deuterium. The cations were characterized by collisionally-activated dissociation (CAD) spectra (Figs. 1–4). Ion **1**$^+$ dissociated upon collisional activation to form H_2N–CH=C=$O^{+\bullet}$ (*m/z* 57) by loss of OH$^\bullet$, HN=CH–C=O^+ (*m/z* 56) by loss of H_2O, H_2N–CH–OH^+ (*m/z* 46) by loss of CO, $COOH^+$ (*m/z* 45) by loss of NH_2CH, H_2N–C-$H^{+\bullet}$ (*m/z* 29), and HC≡NH^+ (*m/z* 28) (Fig. 1a). The ion assignments were made on the basis of the CAD spectrum of [**1**-D_3]$^+$ which showed appropriate mass shifts (Fig. 1b) due to losses of OD (*m/z* 59),

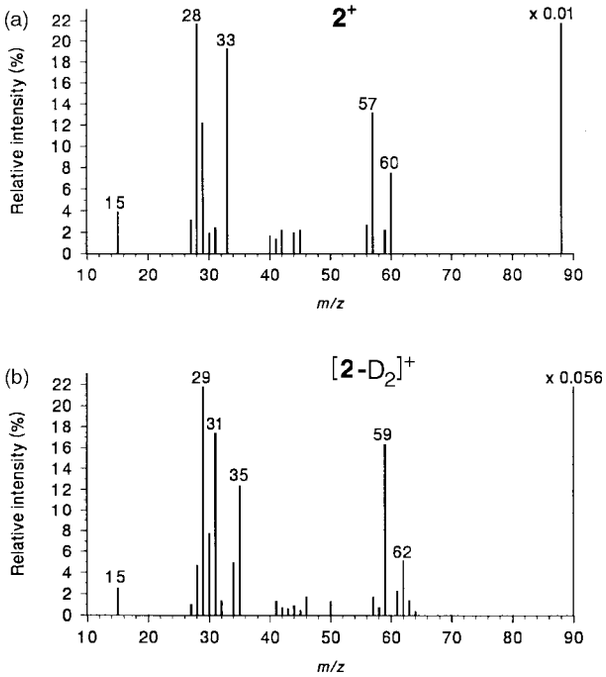

Fig. 2 Collisionally-activated spectrum of (a) $\mathbf{2}^+$, (b) $[\mathbf{2}\text{-}D_2]^+$. The ion relative intensities were normalized to the sum of CAD intensities.

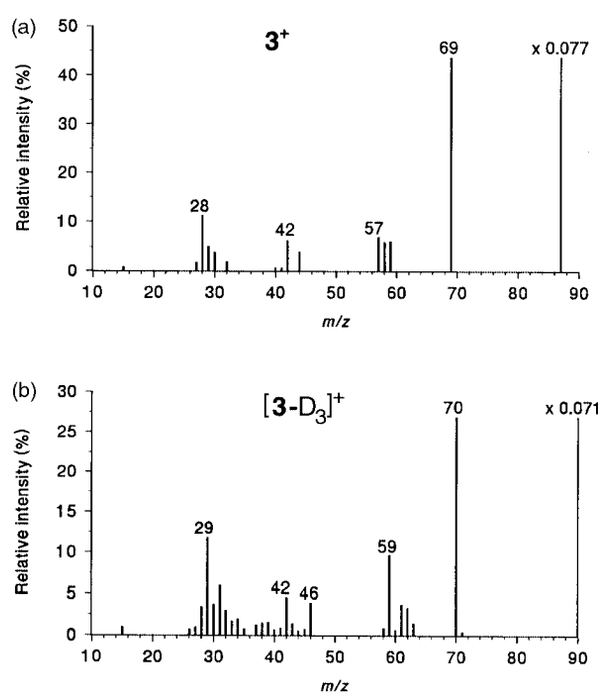

Fig. 3 Collisionally-activated spectrum of (a) $\mathbf{3}^+$, (b) $[\mathbf{3}\text{-}D_3]^+$. The ion relative intensities were normalized to the sum of CAD intensities.

D_2O (*m/z* 57), CO (*m/z* 49), D_2NCH (*m/z* 46), COOD (*m/z* 31), and DCOOD (*m/z* 29). The purity of $\mathbf{1}^+$ was checked by high-resolution mass spectrum which showed that the peak at *m/z* 74 consisted of 98.5% $C_2H_4NO_2^+$ (measured 74.0236, calc. 74.0242) and 1.5% $C_6H_2^{+\bullet}$ (measured 74.0155, calc. 74.0156). The $[\mathbf{1}\text{-}D_3]^+$ ion at *m/z* 77 was accompanied by ~30% of the isobaric $C_6H_5^+$ ion due to fragmentation in the benzyl group. The latter contributed fragments at *m/z* 50 and 51 which appeared in the CAD spectrum of $[\mathbf{1}\text{-}D_3]^+$ (Fig. 1b).

Ion $\mathbf{1}^+$ prepared from phenylalanine appears to differ from the ion prepared recently by O'Hair *et al.* by hydrogen atom loss from the glycine cation radical. CAD of the latter ion showed abundant fragments at *m/z* 58 and 30 which were absent in the CAD spectrum of $\mathbf{1}^+$. Since the loss of H from glycine cation-

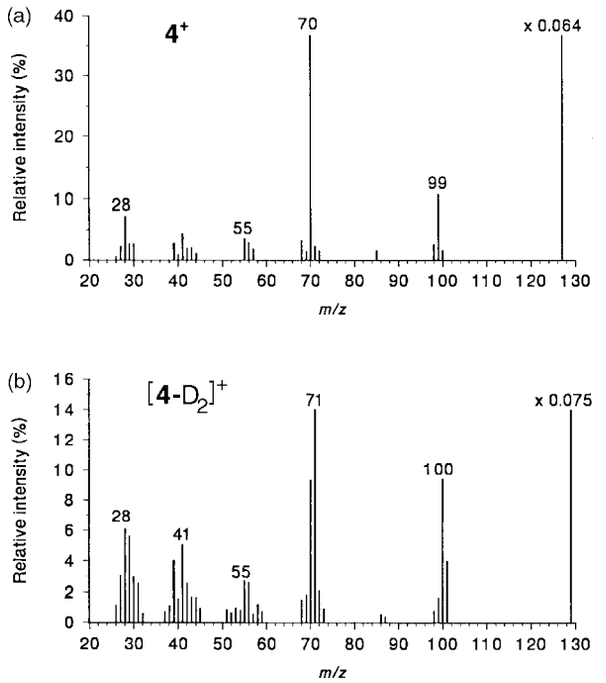

Fig. 4 Collisionally-activated spectrum of (a) $\mathbf{4}^+$, (b) $[\mathbf{4}\text{-}D_2]^+$. The ion relative intensities were normalized to the sum of CAD intensities.

radicals formed with 70 eV electron ionization may not be completely regiospecific, it is possible that the ion reported by O'Hair *et al.* contained isomers other than $\mathbf{1}^+$ that gave rise to the additional fragments in the CAD spectrum.[45]

The CAD spectrum of ion $\mathbf{2}^+$ showed dissociations that were analogous to those of $\mathbf{1}^+$ and formed $H_2N\text{–}CH\text{–}OCH_3^+$ (*m/z* 60) by loss of CO, $H_2N\text{–}CH{=}C{=}O^{+\bullet}$ (loss of OCH_3, *m/z* 57), $H_2N\text{–}CH^{+\bullet}$ (*m/z* 29) by loss of $COOCH_3$, and $HC{\equiv}NH^+$ (*m/z* 28) by elimination of $HCOOCH_3$ (Fig. 2a). The fragmentations showed appropriate mass shifts due to the presence of the amine deuterium atoms in $[\mathbf{2}\text{-}D_2]^+$ (Fig. 2b). In addition, CAD of $\mathbf{2}^+$ produced an abundant $CH_3OH_2^+$ ion (Fig. 2a). The latter dissociation involved mostly but not exclusively a transfer of two hydrogen atoms from the amino group (Fig. 2b). Formation of $CH_3OH_2^+$ and $CH_3OD_2^+$ were the dominant dissociations of metastable $\mathbf{2}^+$ and $[\mathbf{2}\text{-}D_2]^+$, respectively.

The CAD spectrum of ion $\mathbf{3}^+$ showed a prominent peak due to loss of water (*m/z* 69) which represented the only dissociation of metastable $\mathbf{3}^+$. Deuterium labeling (Fig. 3b) revealed that both hydrogens in the water molecule eliminated originated cleanly from the exchangeable amine and/or amide positions. The other CAD peaks were due to eliminations of CO (*m/z* 59), NH_2CH (*m/z* 58), and CH_3NH (*m/z* 57), and formations of fragments at *m/z* 44, 42, and 28–30 (Fig. 3a). The peak at *m/z* 44 shifted to *m/z* 46 in the CAD spectrum of $[\mathbf{3}\text{-}D_3]^+$, indicating retention of the terminal ND_2 group (Fig. 3b). In contrast, the *m/z* 42 peak showed no deuterium content and appeared at *m/z* 42 in the CAD spectrum of $[\mathbf{3}\text{-}D_3]^+$. These dissociations of $\mathbf{3}^+$ can be rationalized by an unusual methyl migration from the methylamino group onto the C-2 carbocation center, followed by elimination of O=C=NH or ethylamine (Scheme 3).

CAD of ion $\mathbf{4}^+$ showed a dominant loss of CO and HN=CH (*m/z* 99) and formation of a pyrrolidyl ion at *m/z* 70 (Fig. 4a). Both these dissociations also appeared in the metastable-ion spectra of $\mathbf{4}^+$. Deuterium labeling in $[\mathbf{4}\text{-}D_2]^+$ showed retention of one or two amine deuterons in the *m/z* 99 ion (Fig. 4b). Interestingly, the pyrrolidyl ion at *m/z* 70 contained in part one deuterium atom from the ND_2 group. This indicated that the pyrrolidyl group was not lost by simple cleavage of the C–N bond, but exchanged protons with the NH_2 group in the course of the elimination.

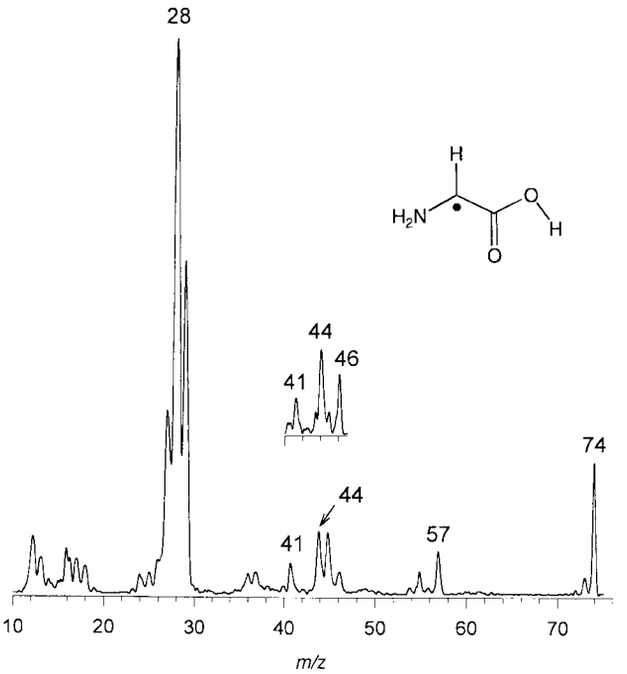

Fig. 5 Neutralization (CH_3SSCH_3, 70% transmittance)–reionization (O_2, 70% transmittance) mass spectrum of $\mathbf{1}^+$. Inset shows the *m*/*z* 40–46 group in the NR mass spectrum of $[\mathbf{1}\text{-}D_3]^+$.

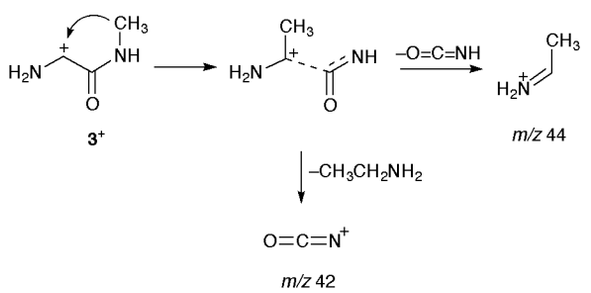

Scheme 3

Radical formation and dissociations

Neutralization of $\mathbf{1}^+$ followed by reionization provided the NR mass spectrum shown in Fig. 5. The spectrum exhibited a moderately abundant survivor ion which indicated that the intermediate radical **1** did not dissociate completely on the 4.1 μs timescale. A possible caveat in assigning the *m*/*z* 74 peak to survivor $\mathbf{1}^+$ was due to the fact that the electron impact spectrum of phenylalanine formed a minor $C_6H_2^{+\bullet}$ ion at *m*/*z* 74 which was isobaric with $\mathbf{1}^+$ (*vide supra*).[31] A reference $C_6H_2^{+\bullet}$ ion was therefore prepared from 1,2,4,5-tetrachlorobenzene and its NR mass spectrum was measured (spectrum not shown). NR of $C_6H_2^{+\bullet}$ produced a survivor ion and signature fragments of C_4H (*m*/*z* 49), C_3H (*m*/*z* 37), C_3 (*m*/*z* 36), and C_2 (*m*/*z* 24). Note that fragments containing C_3 and C_4 cannot be formed from $\mathbf{1}^+$. Fig. 5 showed that these ions were present as very minor peaks in the NR mass spectrum of $\mathbf{1}^+$, indicating some contamination (Fig. 5). After appropriate scaling and spectra subtraction, it can be concluded that <20% of the survivor peak at *m*/*z* 74 could be assigned to contamination by $C_6H_2^{+\bullet}$. This confirmed unambiguously that a fraction of stable **1** (or an isomer) was formed by collisional neutralization of $\mathbf{1}^+$. We note that the charge reversal spectrum of a [glycine − H]$^-$ anion also indicated the presence of a stable radical intermediate as recently reported by O'Hair *et al.*[45]

The dissociations of **1** upon NR gave rise to prominent peaks of HCN, CO, H_2CN, NH_2–C–H and H_2N–CH=C=O. The NR spectrum of $[\mathbf{1}\text{-}D_3]^+$ showed overlapping mass shifts of the *m*/*z* 27–29 group to *m*/*z* 27–31 due to the formation of HCN, CO, DNCH and D_2NCH. The *m*/*z* 44 peak in the spectrum of **1** showed no mass shift due to deuterium, indicating that it belonged to CO_2. The *m*/*z* 45 peak shifted to *m*/*z* 46, indicating the formation of COOH and COOD, respectively (Fig. 5, inset). The aminoketene peak at *m*/*z* 57 retained cleanly two amine deuterons when formed from $[\mathbf{1}\text{-}D_3]^+$, indicating a loss of an intact OD group. It should be noted that the ion and neutral dissociations gave rise to overlapping product peaks in the NR spectra of both $\mathbf{1}^+$ and $[\mathbf{1}\text{-}D_3]^+$. Thus, the contributions of ion and neutral dissociations could not be deconvoluted unambiguously even with the use of isotope labeling. An exception was the H_2O peak in the NR mass spectrum of **1** (Fig. 5) which indicated clearly a neutral dissociation accompanied by hydrogen rearrangement in the radical.

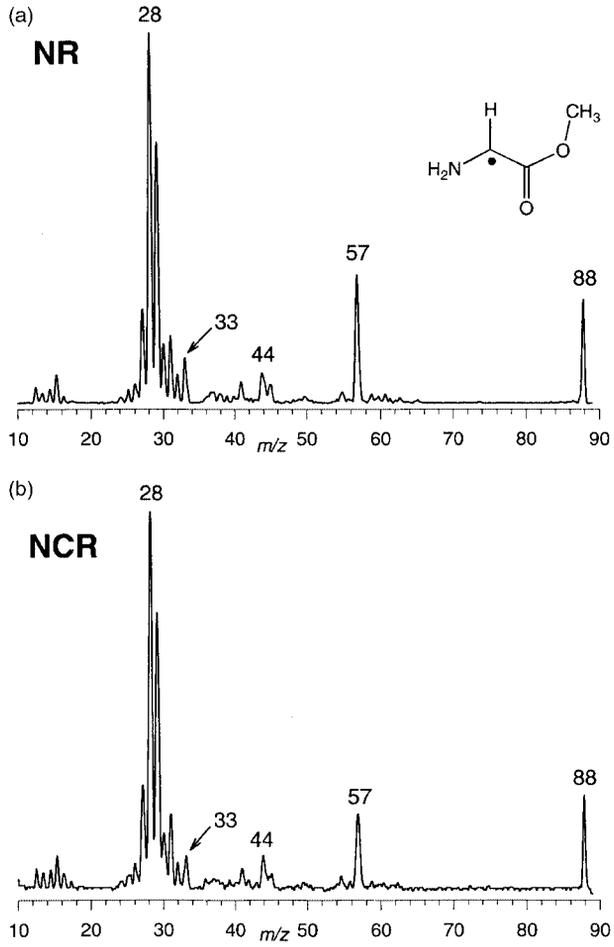

Fig. 6 (a) Neutralization (CH_3SSCH_3, 70% transmittance)–reionization (O_2, 70% transmittance) mass spectrum of $\mathbf{2}^+$. (b) Neutralization (CH_3SSCH_3, 70% transmittance)–collisional activation (He, 50% transmittance)–reionization (O_2, 70% transmittance) mass spectrum of $\mathbf{2}^+$.

A stable survivor ion was also obtained by NR of the methyl ester ion $\mathbf{2}^+$. In this case, the fragmentation of the phenylalanine methyl ester precursor formed no isobaric contaminants, so that the survivor peak at *m*/*z* 88 was unambiguously assigned to ionization of radical **2** or an isomer. The dissociations of **2** involved loss of $CH_3O^\bullet$ to form aminoketene which gave rise to the *m*/*z* 57 peak following reionization (Fig. 6a). The complementary peak at *m*/*z* 31 was also present due to ionization of $CH_3O^\bullet$. The NR mass spectrum of **2** was dominated by small fragments at *m*/*z* 28 and 29, which probably corresponded to combinations of CO, HN=CH and NH_2=CH, by analogy with the NR spectrum of **1**, and to dissociation products of reionized CH_3O^+, which is unstable as a singlet ion.[46,47] Collisional activation of intermediate radicals **2** (Fig. 6b) resulted in an increased formation of low-mass fragments. Interestingly, the $[NH_2CH{=}C{=}O]^{+\bullet}/[\mathbf{2}]^+$ ratio slightly *decreased* upon collisional activation of the neutral intermediates, indicat-

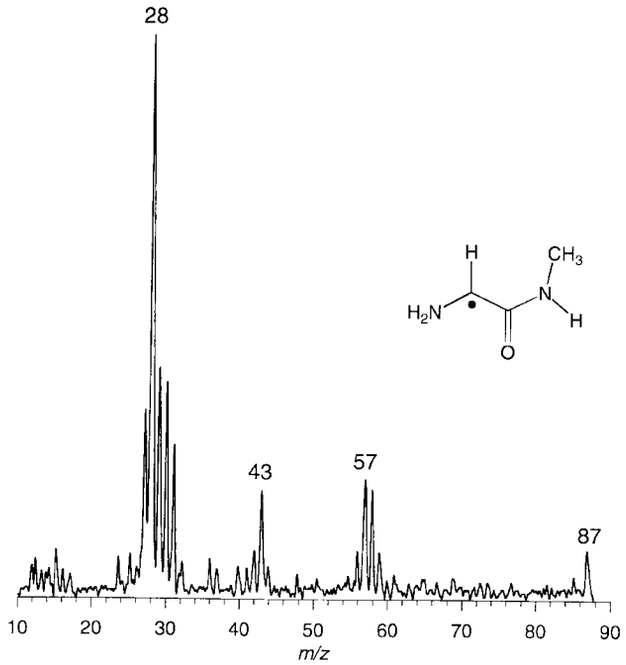

Fig. 7 Neutralization (CH_3SSCH_3, 70% transmittance)–reionization (O_2, 70% transmittance) mass spectrum of $\mathbf{3}^+$.

ing that the aminoketene molecule or cation-radical were more susceptible to further dissociations than **2**/$\mathbf{2}^+$.

A weak survivor ion at *m*/*z* 87 was obtained by NR of the methylamide ion $\mathbf{3}^+$ (Fig. 7). Since there were no isobaric overlaps at *m*/*z* 87 in the electron impact spectrum of phenylalanine *N*-methylamide, the survivor peak could be unambiguously assigned to reionized radical **3** or an isomer. The NR dissociations of **3** showed a pattern that differed from that in the CAD spectrum of $\mathbf{3}^+$ (*cf*. Fig. 3a,b). In particular, elimination of water was absent in the NR mass spectrum, indicating that it must have corresponded entirely to an ion dissociation. Note also that the peak of water was absent in the NR mass spectrum of $\mathbf{3}^+$, indicating that ion neutralization was not accompanied by CAD. The NR mass spectrum showed formations of *m*/*z* 58 (loss of NH_2CH), *m*/*z* 57 (loss of CH_3NH) and *m*/*z* 43 (loss of CH_3CHNH_2). Also, a peak of methylamine at *m*/*z* 31 was observed which was absent in the CAD spectrum. The formation of neutral HN=C=O and CH_3NH_2 pointed to rearrangements in dissociating radical **3**. The former can be accounted for by a methyl migration, followed by a CH–C=O bond cleavage. The formation of methylamine and its complementary fragment at *m*/*z* 56 must be due to a hydrogen transfer, which is depicted in Scheme 4.

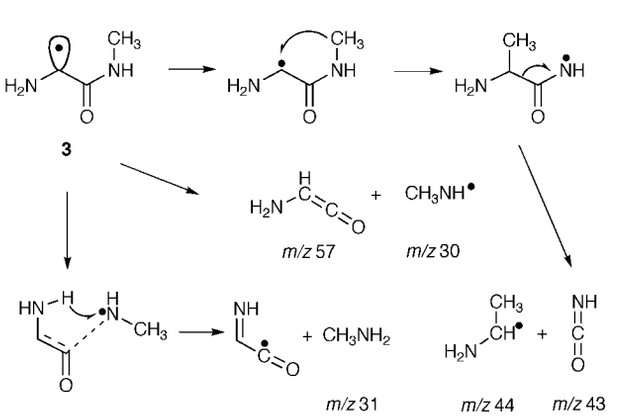

Scheme 4

Cation structures and dissociation energies

Geometry optimizations with B3LYP/6-31+G(d,p) yielded four stable conformers of ion $\mathbf{1}^+$, *anti-syn*-$\mathbf{1}^+$, *syn-syn*-$\mathbf{1}^+$, *anti-anti*-$\mathbf{1}^+$, and *gauche-anti*-$\mathbf{1}^+$ in order of decreasing stability (Fig. 8, Table 1). The relative stabilities of the cationic conformers were mainly determined by the orientation of the $C^+{=}O^-$ and $O^-{-}H^+$ bond dipoles, which was more favorable in the *syn*-conformers *anti-syn*-$\mathbf{1}^+$ and *syn-syn*-$\mathbf{1}^+$. The orientation of the C–N and C–OH bonds was less important, although the *anti* conformation appeared to be slightly more favorable (Table 1). Recent MP2/6-31+G(d) calculations of O'Hair *et al*. found a reversed order of stability for *anti-syn*-$\mathbf{1}^+$ and *syn-syn*-$\mathbf{1}^+$ whereby the latter was 4.6 kJ mol^{-1} more stable.[45] We note that in our calculations *anti-syn*- $\mathbf{1}^+$ was consistently 8–10 kJ mol^{-1} more stable than *syn-syn*-$\mathbf{1}^+$ at all levels of theory including B3LYP/6-31+G(d,p) and 6-311+G(2df,p), MP2/6-311G(d,p), 6-311+G(2df,p), and 6-311+G(3df,2p), and QCISD(T)/6-311G(d,p).

The lowest-threshold energy dissociation of $\mathbf{1}^+$ was elimination of CO to yield protonated formamide, $H_2N{-}CH{-}OH^+$, which was mildly exothermic (Table 1). The elimination was thought to proceed *via* an acylium intermediate, $H_2N{-}CH(OH){-}C{\equiv}O^+$ ($\mathbf{5}^+$). However, attempted geometry optimization of structure $\mathbf{5}^+$ resulted in a dissociation yielding an ion–molecule complex of $H_2N{-}CH{-}OH^+$ with CO which was bound against dissociation by a mere 31 kJ mol^{-1} . Since ion $\mathbf{1}^+$ was stable, the elimination of CO must have overcome a substantial barrier that stabilized $\mathbf{1}^+$ *kinetically*. Other dissociations of $\mathbf{1}^+$ were substantially endothermic as summarized in Table 1.

The optimized structures of ions $\mathbf{2}^+$ and $\mathbf{3}^+$ are shown in Fig. 9. The calculated bond lengths in the glycyl moieties of $\mathbf{2}^+$ and $\mathbf{3}^+$ were similar to those in *anti-syn*-$\mathbf{1}^+$. Other conformers of $\mathbf{2}^+$ and $\mathbf{3}^+$ have not been investigated. The dissociation energetics of $\mathbf{2}^+$ and $\mathbf{3}^+$ were studied computationally at the combined B3LYP and MP2 levels of theory. We have shown previously that empirical averaging of B3LYP and spin-projected (PMP2) relative energies provided mostly, albeit not uniformly, an improved fit with reference G2(MP2) or experimental data.[48,36d] Averaged relative energies are therefore discussed in the text; the relative energies obtained at the various levels of theory are given in Table 1.

Elimination of CO from $\mathbf{2}^+$ was calculated to be substantially *exothermic*, $\Delta H_{r,0} = -59$ kJ mol^{-1} (Table 1). The fact that $\mathbf{2}^+$ was stable must therefore have been due to an energy barrier to $CH_3O^{\bullet}$ migration. By analogy with the homologous ion $\mathbf{5}^+$ (*vide supra*) and with regard to the exothermic CO expulsion, we presumed that a putative $H_2N{-}CH(OCH_3){-}C{\equiv}O^+$ intermediate was unbound. The main dissociation of metastable $\mathbf{2}^+$, formation of $CH_3OH_2^+$, could produce azirinone or (HCN + CO) as neutral products. The calculated threshold energies favored the latter ($\Delta H_{r,0}$ = 144 kJ mol^{-1}, Table 1). However, the formation of $CH_3OH_2^+$ must have proceeded with hydrogen rearrangements which were likely to have activation energies. The abundant CAD formation of $HC{\equiv}NH^+$ by loss of CH_3OH and CO required 183 kJ mol^{-1} at threshold. In contrast, a direct cleavage of the C–O bond to eliminate $CH_3O^{\bullet}$ was substantially endothermic, $\Delta H_{r,0}$ = 316 kJ mol^{-1}. Note that loss of the methoxy radical was an important dissociation of $\mathbf{2}^+$ upon collisional activation (Fig. 2).

The elimination of water from $\mathbf{3}^+$, which was the main dissociation of metastable $\mathbf{3}^+$, was calculated to require 149 kJ mol^{-1} at the threshold. The formation of $HC{\equiv}NH^+$ by loss of methyl amine and CO, which was only moderately abundant in the CAD spectrum of $\mathbf{3}^+$, required 255 kJ mol^{-1}. Note that both dissociations proceeded with hydrogen rearrangements which likely involved activation energies.

Radical structures and dissociation energies

Four structures were calculated for $H_2N{-}CH{-}COOH^{\bullet}$ with B3LYP/6-31+G(d,p) to be local energy minima, *e.g.* in the order of decreasing stability, *anti-syn*-**1**, *syn-syn*-**1**, *anti-anti*-**1**,

Table 1 Relative and dissociation energies of glycol cations $\mathbf{1}^+$–$\mathbf{3}^+$

Ion	Relative energy[a] B3LYP/ 6-31+G(d,p)	B3LYP/ 6-311+G(2df,p)		MP2/ 6-311+G(2df,p)	G2(MP2)
anti-syn-$\mathbf{1}^+$	0	0	0[b]	0	0
anti-syn-$\mathbf{1}^+$ (VI)[c]		50	49	48	
syn-syn-$\mathbf{1}^+$	7	8	8	9	9
anti-anti-$\mathbf{1}^+$	41	38	39	40	36
gauche-anti-$\mathbf{1}^+$	56	51	57	62	57
H_2N–CH(OH)$\cdots$$CO^+$ ($\mathbf{5}^+$)	−29	−36	−38	−40	
H_2N–CH–OH^+ + CO	1	−6	−4	−3	−13
$HC{\equiv}NH^+$ + CO + H_2O	220	204	192	180	175
$HC{\equiv}NH^+$ + HCOOH	175	165	159	153	160
H_2N–CH=C=$O^{+\bullet}$ + $OH^\bullet$	374	366	385	403	404
H_2N–C–H + $COOH^+$	438	419	425	431	424
H_2N–C–$H^{+\bullet}$ + $COOH^\bullet$	424	422	436	450	444
anti-anti-$\mathbf{2}^+$	0	0	0	0	
H_2N–CH–OCH_3^+ + CO	−57	−61	−59	−57	
H_2N–CH=C=$O^{+\bullet}$ + OCH_3	294	287	316	345	
$CH_3OH_2^+$ + CO + HCN	163	155	144	133	
$HC{\equiv}NH^+$ + CH_3OH + CO	206	192	183	174	
$CH_3OH_2^+$ + cyc-O=C–N=CH	294	295	294	292	
anti-anti-$\mathbf{3}^+$	0	0	0	0	
H_2N–CH–$NHCH_3^+$ + CO	−51	−58	−56	−54	
HN=CH–C=NCH_3 + H_2O	160	150	149	148	
$HC{\equiv}NH^+$ + CO + CH_3NH_2	282	263	255	247	

[a] In kJ mol^{-1} at 0 K, including B3LYP/6-31+G(d,p) zero-point corrections. [b] Averaged B3LYP and PMP2/6-311+G(2df,p) energies. [c] Vertical ionization of **1**.

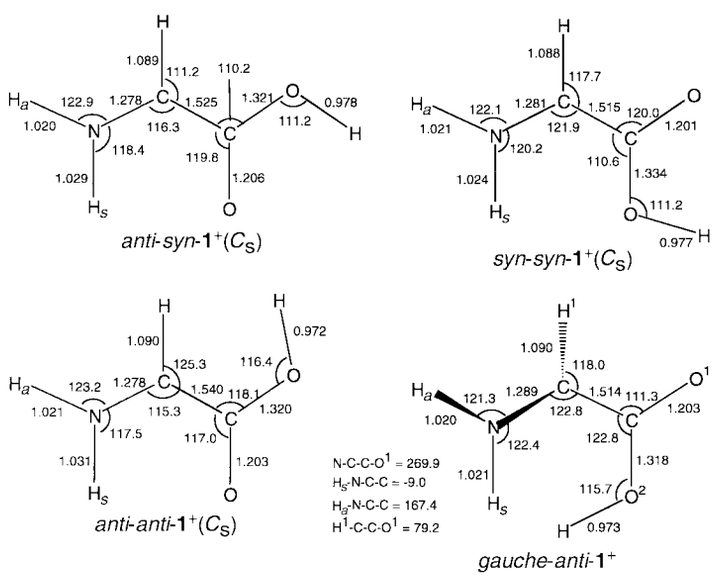

Fig. 8 B3LYP/6-31+G(d,p) optimized structures of ion conformers $\mathbf{1}^+$. Bond lengths in ångstroms, bond and dihedral angles in degrees.

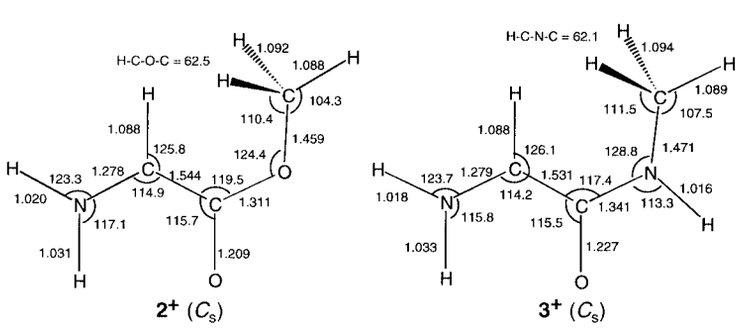

Fig. 9 B3LYP/6-31+G(d,p) optimized structures of $\mathbf{2}^+$ and $\mathbf{3}^+$. Bond lengths in ångstroms, bond and dihedral angles in degrees.

and *gauche-anti*-**1** (Fig. 10). Similar to the conformers of $\mathbf{1}^+$, the radical conformers in which the C^+=O^- and O^-–H^+ bond dipoles were *syn*-oriented were more stable than the *anti*-ones. A valence-bond isomer (H_2N–CH(OH)–C=O$^\bullet$, **5**, Fig. 11) was also found to be a bound structure, which was 121 kJ mol^{-1} less stable than *anti-syn*-**1** (Table 2). In addition, *anti-syn*-**1** and **5** were separated by a large energy barrier to isomerization, E_a = 310 kJ mol^{-1} relative to *anti-syn*-**1**. The transition state

Table 2 Relative and dissociation energies of glycyl radicals **1**–**3**

Radical	Relative energy[a]				
	B3LYP/ 6-31+G(d,p)	B3LYP/ 6-311+G(2df,p)		MP2/ 6-311+G(2df,p)	G2(MP2)
anti-syn-**1**	0	0	0[b]	0	0
anti-syn-**1** (VN)[c]		39	39	39	
syn-syn-**1**	5	6	6	5	6
anti-anti-**1**	26	23	23	24	21
gauche-anti-**1**	46	44	45	45	40
H_2N–CH(OH)–CO$^{\bullet}$ (**5**)	143	145	139	132	121
TS (**1**→**5**)	286	278	307	335	310
H_2N–CH–OH$^{\bullet}$ + CO	161	155	152	150	129
HN=CH–COOH + H$^{\bullet}$	233	228	210	191	198
TS**6**	234	230	223	216	207
H_2N–CH=C=O + OH$^{\bullet}$	324	316	324	333	316
H_2N–C–H + COOH$^{\bullet}$	334	328	339	350	324
2	0	0	0	0	
HN=CH–C=O$^{\bullet}$ + CH_3OH	166	166	174	181	
H_2N–CH=C=O + $CH_3O^{\bullet}$	240	233	253	273	
H_2N–C–H + $COOCH_3^{\bullet}$	294	291	304	317	
$COOCH_3^{\bullet}$ → CO + $OCH_3^{\bullet}$	68	67	78	89	
3	0	0	0	0	
H_2N–CH(CH_3)–CO–NH$^{\bullet}$ (**7**)	103	108	108	108	
H_2N–CH–$CH_3^{\bullet}$ + O=C=NH	68	52	55	58	
H_2N–CH–$NHCH_3^{\bullet}$ + CO	143	137	135	133	
HN=CH–C=O$^{\bullet}$ + CH_3NH_2	190	187	188	188	
H_2N–CH=C=O + $CH_3NH^{\bullet}$	251	240	253	267	
H_2N–C–H + CH_3NH–C=O$^{\bullet}$	286	282	297	312	
HN=CH–C=O$^{\bullet}$ → HN=CH$^{\bullet}$ + CO	29	21	18	15	

[a] In kJ mol^{-1} at 0 K, including B3LYP/6-31+G(d,p) zero-point corrections. [b] Averaged B3LYP and PMP2/6-311+G(2df,p) energies. [c] Vertical neutralization of $\mathbf{1}^+$.

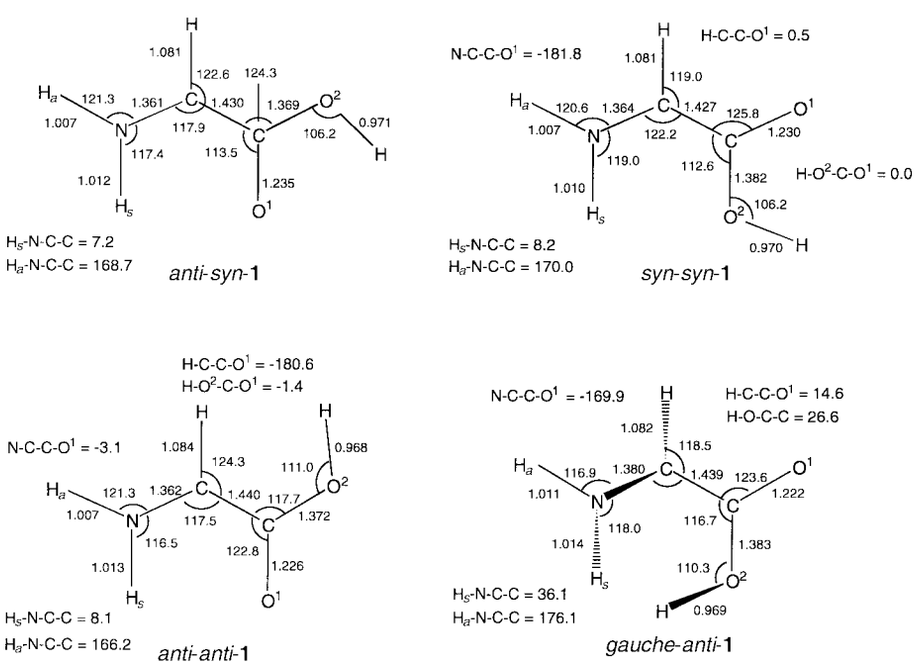

Fig. 10 B3LYP/6-31+G(d,p) optimized structures of radical conformers **1**. Bond lengths in ångstroms, bond and dihedral angles in degrees.

geometry (**TS(1→5)**) is shown in Fig. 11. Elimination of CO was the lowest-energy dissociation of *anti-syn*-**1** (Table 2). Simple bond cleavage dissociations to form H_2N–C–H and COOH$^{\bullet}$, H_2N–CH=C=O and OH$^{\bullet}$, and HN=CH–COOH and H$^{\bullet}$ were more endothermic. The reaction coordinate for the latter reaction was investigated by stepwise calculations and found to have a transition state (**TS6**, Fig. 11) which was 10 kJ mol^{-1} above the energy of the products at 0 K. In contrast, the dissociation of the C–O bond in *anti-syn*-**1** was continuously endothermic according to B3LYP/6-31+G(d,p) calculations. No substantial activation barrier was therefore expected for the reverse addition of OH$^{\bullet}$ to aminoketene.

The optimized structures of radicals **2** and **3** are shown in Fig. 12. The bond lengths and angles in the glycyl moieties of **2** and **3** were similar to those in *anti-syn*-**1**. The energetics of radicals **2** and **3** were investigated with combined B3LYP and PMP2/6-311+G(2df,p) calculations for the most important dissociations observed in the NR mass spectra (Table 2). Elimination of methanol was the lowest-energy dissociation of **2** requiring 166 kJ mol^{-1} at the product threshold. How-

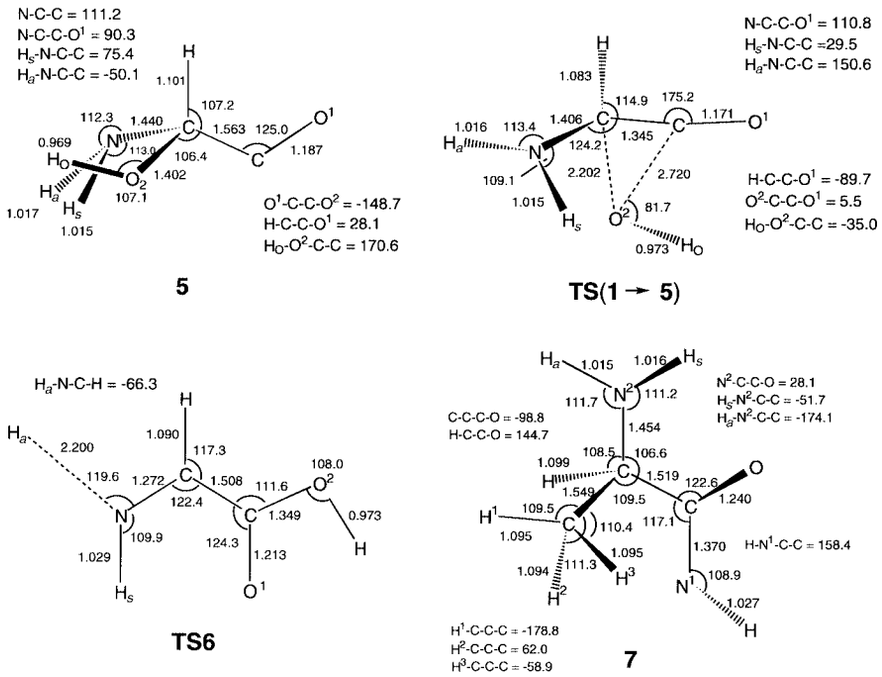

Fig. 11 B3LYP/6-31+G(d,p) optimized structures of radical intermediates and transition states. Bond lengths in ångstroms, bond and dihedral angles in degrees.

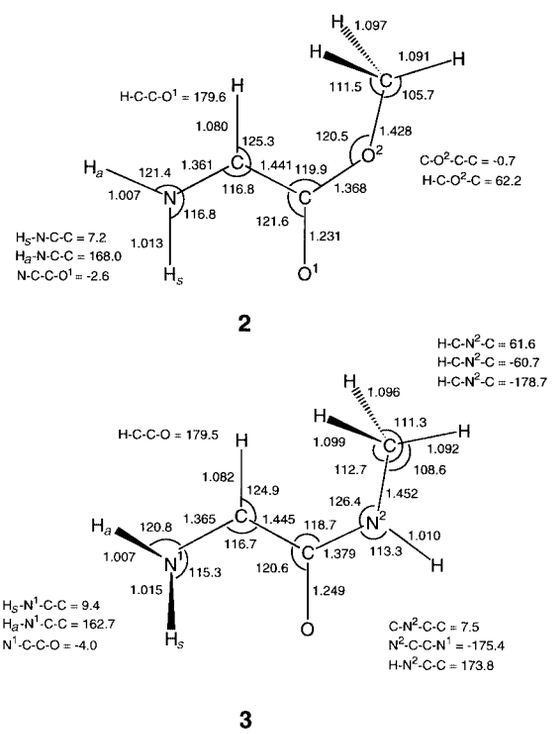

Fig. 12 B3LYP/6-31G(d,p) optimized structures of radicals **2** and **3**. Bond lengths in ångstroms, bond and dihedral angles in degrees.

ever, methanol elimination must have proceeded with a hydrogen rearrangement which was likely to involve an activation energy. Loss of $CH_3O^{\bullet}$ from **2** was 273 kJ mol^{-1} endothermic, whereas a C–C bond cleavage yielding H_2N–C–H and $COOCH_3$ required 317 kJ mol^{-1} threshold energy. Accordingly, both aminocarbene (*m*/*z* 29) and aminoketene (*m*/*z* 57) were prominent products on the NR mass spectrum. The low relative intensity of $COOCH_3$ (*m*/*z* 59) can be explained by its low dissociation energy to CO and $OCH_3^{\bullet}$ (78 kJ mol^{-1}, Table 2). The very low relative intensity of HN=CH–C=O$^+$ (*m*/*z* 56) by reionization of HN=CH–C=O$^{\bullet}$ can be likewise explained by the low stability of the intermediate radical which was bound by only 18 kJ mol^{-1} against dissociation to HC=NH$^{\bullet}$ and CO (Table 2).

Elimination of HN=C=O to yield CH_3CH–$NH_2^{\bullet}$ was the lowest-energy dissociation of radical **3** ($\Delta H_{r,0} = 55$ kJ mol^{-1}). However, the elimination was accompanied by methyl migration (Scheme 4) and therefore must have involved an intermediate (**7**) and/or an additional activation barrier. The optimized structure of putative radical intermediate **7** is shown in Fig. 11. Radical **7** was calculated to be 108 kJ mol^{-1} less stable than **3**, which placed it 53 kJ mol^{-1} above the dissociation threshold for CH_3CH–$NH_2^{\bullet}$ and O=C=NH. The fact that **7** was a bound structure must therefore be due to a potential energy barrier to dissociation of the C–C=O bond. Another rearrangement resulting in elimination of CH_3NH_2 was more endothermic, $\Delta H_{r,0} = 188$ kJ mol^{-1} (Table 2). Direct bond dissociations of **3** to form $CH_3NH^{\bullet}$ and NH_2–CH=C=O, and H_2N–C–H and $CH_3NHCO^{\bullet}$ were substantially more endothermic and required 253 and 297 kJ mol^{-1}, respectively (Table 2).

In summarizing the energetics of neutral dissociations it may be noted that simple bond dissociations were somewhat less endothermic in **2** and **3** than in **1**. Consistent with this finding, the relative abundance of reionized H_2N–CH=C=O$^{+\bullet}$ was greater in the NR mass spectra of **2** and **3** compared with that of **1**.

Conclusions

Glycine-derived radicals 2-glycyl, 2-glycyl methyl ester and 2-glycyl *N*-methylamide were generated from the corresponding cations and found to yield fractions of stable species in the gas phase. Both simple bond cleavages and rearrangements due to hydrogen and heavy-atom migrations were observed for the radical unimolecular dissociations. G2(MP2) *ab initio* calculations for the simplest 2-glycyl radical and combined B3LYP and PMP2 calculations for 2-glycyl methyl ester and 2-glycyl *N*-methylamide radicals indicated that unimolecular dissociations were high-energy processes that would be slow in thermal radicals. It is therefore concluded that in the condensed phase the radicals would preferentially undergo bimolecular reactions, such as hydrogen abstraction from a suitable donor.[20]

Acknowledgements

Support by the National Science Foundation (Grants CHE-9712750 and CHE-9808182) is gratefully acknowledged. We also thank Dr Martin Sadilek and Jill K. Wolken for technical assistance.

References

1 For a recent comprehensive review see: J. Stubbe and W. A. van der Donk, *Chem. Rev.*, 1998, **98**, 705.
2 B. M. Sjoberg, P. Reichard, A. Graslund and A. Ehrenberg, *J. Biol. Chem.*, 1977, **252**, 536.
3 B. A. Barry, M. K. El-Deeb, P. O. Sandusky and G. Babcock, *J. Biol. Chem.*, 1990, **265**, 20139.
4 R. Karthein, R. Dietz, W. Nastainczyk and H. H. Ruf, *Eur. J. Biochem.*, 1988, **171**, 313.
5 J. E. Huyett, P. E. Doan, R. Gurbiel, A. L. P. Houseman, M. Sivaraja, D. B. Goodin and B. M. Hoffman, *J. Am. Chem. Soc.*, 1995, **117**, 9033.
6 W. S. McIntyre, D. E. Wemmer, A. Chistoserdov and M. E. Lindstron, *Science*, 1991, **252**, 817.
7 L. Chen, F. S. Matthews, V. L. Davidson, E. G. Huizenga, F. M. D. Vellieux, J. A. Duine and W. G. J. Hol, *FEBS Lett.*, 1991, **287**, 163.
8 J. Knappe, F. A. Neugebauer, H. P. Blaschkowski and M. Ganzler, *Proc. Natl. Acad. Sci. USA*, 1984, **81**, 1332.
9 C. V. Parast, K. K. Wong, S. A. Lewisch and J. W. Kozarich, *Biochemistry*, 1995, **34**, 2393.
10 X. Sun, J. Harder, M. Krook, B.-M. Sjoberg and P. Reichard, *Proc. Natl. Acad. Sci. USA*, 1993, **90**, 577.
11 E. Mulliez, M. Fontecave, J. Gaillard and P. Reichard, *J. Biol. Chem.*, 1993, **268**, 2296.
12 X. Sun, B. Eliasson, J. Pontis, J. Andersson, G. Buist, B.-M. Sjoberg and P. Reichard, *J. Biol. Chem.*, 1995, **270**, 2443.
13 R. Zhao, J. Lind, G. Merenyi and T. E. Eriksen, *J. Am. Chem. Soc.*, 1994, **116**, 12010.
14 G. T. Babcock, M. Espe, C. Hoganson, N. Lydakis-Simantiris, J. McCracken, W. Shi, S. Styring, C. Tommos and K. Warncke, *Acta Chem. Scand.*, 1997, **51**, 533.
15 C. J. Bender, M. Sahlin, G. T. Babcock, B. A. Barry, T. K. Chandrasekhar, S. P. Salowe, J. Stubbe, B. Lindstrom, L. Petterson, A. Ehrenberg and B.-M. Sjoberg, *J. Am. Chem. Soc.*, 1989, **111**, 8076.
16 D. Yu, A. Rauk and D. A. Armstrong, *J. Am. Chem. Soc.*, 1995, **117**, 1789.
17 V. Barone, C. Adamo, A. Grand and R. Subra, *Chem. Phys. Lett.*, 1995, **242**, 351.
18 V. Barone, C. Adamo, A. Grand, F. Jolibois, Y. Brunel and R. Subra, *J. Am. Chem. Soc.*, 1995, **117**, 12618.
19 F. Himo and L. A. Eriksson, *J. Chem. Soc.*, *Perkin Trans. 2*, 1998, 305.
20 F. Himo and L. A. Eriksson, *J. Am. Chem. Soc.*, 1998, **120**, 11449.
21 For recent reviews of the technique see: (*a*) C. A. Schalley, G. Hornung, D. Schroder and H. Schwarz, *Chem. Soc. Rev.*, 1998, **27**, 91; (*b*) F. Turecek, *J. Mass Spectrom.*, 1998, **33**, 779; (*c*) N. Goldberg and H. Schwarz, *Acc. Chem. Res.*, 1994, **27**, 347; (*d*) F. Turecek, *Org. Mass Spectrom.*, 1992, **27**, 1087.
22 P. Danis, R. Feng and F. W. McLafferty, *Anal. Chem.*, 1986, **58**, 348.
23 F. Turecek, D. E. Drinkwater and F. W. McLafferty, *Org. Mass Spectrom.*, 1989, **24**, 669.
24 S. A. Shaffer, F. Turecek and R. L. Cerny, *J. Am. Chem. Soc.*, 1994, **116**, 12117.
25 D. W. Kuhns, T. B. Tran, S. A. Shaffer and F. Turecek, *J. Phys. Chem.*, 1994, **98**, 4845.
26 D. W. Kuhns and F. Turecek, *Org. Mass Spectrom.*, 1994, **29**, 463.
27 M. Sadilek and F. Turecek, *J. Phys. Chem.*, 1996, **100**, 224.
28 M. Sadilek and F. Turecek, *J. Phys. Chem.*, 1996, **100**, 9610.
29 M. Sadilek and F. Turecek, *Chem. Phys. Lett.*, 1996, **263**, 203.
30 V. Q. Nguyen, M. Sadilek, A. J. Frank, J. G. Ferrier and F. Turecek, *J. Phys. Chem. A*, 1997, **101**, 3789.
31 F. Turecek, F. H. Carpenter, M. J. Polce and C. Wesdemiotis, *J. Am. Chem. Soc.*, 1999, **121**, 7955.
32 F. Turecek, M. Gu and S. A. Shaffer, *J. Am. Soc. Mass Spectrom.*, 1992, **3**, 493.
33 GAUSSIAN94, (Revision D.1), M. J. Frisch, G. W. Trucks, H. B. Schlegel, P. M. W. Gill, B. G. Johnson, M. A. Robb, J. R. Cheeseman, T. A. Keith, G. A. Petersson, J. A. Montgomery, K. Raghavachari, M. A. Al-Laham, V. G. Zakrzewski, J. V. Ortiz, J. B. Foresman, J. Cioslowski, B. B. Stefanov, A. Nanayakkara, M. Challacombe, C. Y. Peng, P. Y. Ayala, W. Chen, M. W. Wong, J. L. Andres, E. S. Replogle, R. Gomperts, R. L. Martin, D. J. Fox, J. S. Binkley, D. J. Defrees, J. Baker, J. P. Stewart, M. Head-Gordon, C. Gonzalez and J. A. Pople, Gaussian, Inc., Pittsburgh, PA, 1995.
34 A. D. Becke, *J. Chem. Phys.*, 1993, **98**, 1372, 5648.
35 P. J. Stephens, F. J. Devlin, C. F. Chablowski and M. J. Frisch, *J. Phys. Chem.*, 1994, **98**, 11623.
36 See for example: (*a*) C. W. Bauschlicher and H. Partridge, *J. Chem. Phys.*, 1995, **103**, 1788; (*b*) A. J. Frank, M. Sadilek, J. G. Ferrier and F. Turecek, *J. Am. Chem. Soc.*, 1996, **118**, 11321; (*c*) A. J. Frank, M. Sadilek, J. G. Ferrier and F. Turecek, *J. Am. Chem. Soc.*, 1997, **119**, 12343; (*d*) F. Turecek, *J. Phys. Chem. A*, 1998, **102**, 4703.
37 M. W. Wong, *Chem. Phys. Lett.*, 1996, **256**, 391.
38 G. Rauhut and R. Pulay, *J. Phys. Chem.*, 1995, **99**, 3093.
39 J. W. Finley and P. J. Stephens, *J. Mol. Struct.* (*THEOCHEM*), 1995, **357**, 225.
40 A. P. Scott and L. Radom, *J. Phys. Chem.*, 1996, **100**, 16502.
41 C. Møller and M. S. Plesset, *Phys. Rev.*, 1934, **46**, 618.
42 L. A. Curtiss, K. Raghavachari and J. A. Pople, *J. Chem. Phys.*, 1993, **98**, 1293.
43 L. A. Curtiss, K. Raghavachari, P. C. Redfern and J. A. Pople, *J. Chem. Phys.*, 1997, **106**, 1063.
44 K. Raghavachari, B. B. Stefanov and L. A. Curtiss, *J. Chem. Phys.*, 1997, **106**, 6764.
45 R. A. J. O'Hair, S. Blanksby, M. Styles and J. H. Bowie, *Int. J. Mass. Spectrom.*, 1999, **182/183**, 203.
46 P. C. Burgers and J. L. Holmes, *Org. Mass Spectrom.*, 1984, **19**, 452.
47 M. Aschi, J. N. Harvey, C. A. Schalley, D. Schroder and H. Schwarz, *Chem. Commun.*, 1998, 531.
48 F. Turecek and J. L. Wolken, *J. Phys. Chem. A*, 1999, **103**, 1905.

Paper 9/03943K